photonics

MDPI

Communication

Compact, High Extinction Ratio, and Low-Loss Polarization Beam Splitter on Lithium-Niobate-On-Insulator Using a Silicon Nitride Nanowire Assisted Waveguide and a Grooved Waveguide

Jinming Tao [1,2], Xintong Li [1,2], Jinye Li [1], Shuangxing Dai [1], Yiru Zhao [1,2], Chuangchuang Wei [1,2] and Jianguo Liu [1,*]

[1] State Key Laboratory on Integrated Optoelectronics, Institute of Semiconductors, Chinese Academy of Sciences, Beijing 100083, China
[2] College of Materials Science and Opto-Electronic Technology, University of Chinese Academy of Sciences, Beijing 100049, China
* Correspondence: jgliu@semi.ac.cn

Abstract: We propose a compact, high extinction ratio, and low-loss polarization beam splitter (PBS) on a lithium-niobate-on-insulator (LNOI) platform, based on an asymmetrical directional coupler and using a silicon nitride nanowire assisted waveguide (WG) and a grooved WG. By properly designing Si_3N_4 nanowires and grooved LN WGs, TE polarization meets the phase matching condition, while significant mismatching exists for TM polarization. Numerical simulations show that the PBS has an ultra-high extinction ratio (ER) of TE_0 and TM_0 (larger than 40 dB and 50 dB, respectively). The device extinction ratios are larger than 10 dB over 100 nm wavelength ranges. Moreover, the device has an ultra-low insertion loss (IL less than 0.05 dB) at the wavelength of 1550 nm and maintains ILs less than 0.4 dB over 100 nm wavelength ranges.

Keywords: asymmetric directional coupler; lithium-niobate-on-insulator; polarization beam splitter

Citation: Tao, J.; Li, X.; Li, J.; Dai, S.; Zhao, Y.; Wei, C.; Liu, J. Compact, High Extinction Ratio, and Low-Loss Polarization Beam Splitter on Lithium-Niobate-On-Insulator Using a Silicon Nitride Nanowire Assisted Waveguide and a Grooved Waveguide. *Photonics* **2022**, *9*, 779. https://doi.org/10.3390/photonics9100779

Received: 19 September 2022
Accepted: 17 October 2022
Published: 19 October 2022

1. Introduction

Lithium niobate (LN) is known as an excellent optical material in the field of communication technology because of its excellent performance in electro-optic, acousto-optic, and nonlinear optics. Due to the low refractive index difference between the core and cladding ($n < 0.02$), the traditional ion diffusion ln waveguides (WGs) have weak restrictions on the optical field and are difficult to reduce the device size. Thanks to the progress of thin film lithium-niobate (LN) manufacturing technology [1], lithium niobate on insulator (LNOI) can achieve sub-wavelength light limitation, which has broad application prospects for photonic integrated circuits (PIC) [2]. Similar to the other high-index-contrast platforms, LNOI suffers from the polarization-dependent problem due to the birefringence caused by the asymmetrical waveguide structures and the inherent anisotropy property of LN [3]. Therefore, polarization diversity systems are needed to solve these problems in PICs.

Recently, adiabatic coupler [4], Mach Zehnder interferometer [5,6], and subwavelength grating [7] have been used to realize wideband PBS on LNOI platform. However, these PBSs have a large footprint and limited application.

Asymmetric directional coupler (ADC) has been proved to be a simple method to realize compact PBS on other platforms, such as silicon on insulator (SOI) [8]. It is well known that the refractive index difference between fundamental transverse electric mode (TE_0) and fundamental transverse magnetic mode (TM_0) of quasi-single mode silicon WG with a typical thickness of 220 nm is about 0.7. With high birefringence, compact PBS based on the on-chip ADC can be achieved on SOI by using different widths WGs [9–11]. However, LNOI waveguide birefringence is much smaller than SOI [12–14]. For example, the refractive index difference between TE_0 and TM_0 of LN single-mode waveguide with a height of 400 nm is usually less than 0.2. Therefore, this kind of design may not be suitable for LNOI.

Hybrid plasmonic waveguide (HPW) [15,16] is another effective way to enhance birefringence to realize compact PBS [17–19]. Depositing metal on the waveguide can change the refractive index of TM polarization. This design significantly enhances the birefringence of the waveguide, to split TE and TM mode. However, due to the inherent metallic absorption, the insertion loss of HPW is high.

In this paper, we propose a PBS consisted of a silicon nitride nanowire assisted waveguide and a grooved waveguide, which realizes compact, high extinction ratio, and low loss on LNOI platform. Table 1 lists the comparison between LNOI-based PBSs proposed recently and work in this paper. Our device is very competitive, especially in the x-cut platform. Most importantly, we can finely adjust the refractive index of TE mode to achieve a high extinction ratio (>40 dB) of TE mode. Moreover, with the help of silicon nitride nanowires, the refractive index of TM polarization increases significantly, while the refractive index of TM polarization in the grooved waveguide is low [20]. Therefore, when TE polarization meets the phase matching condition, the TM polarization coupling mismatch is large to achieve a high extinction ratio (>50 dB) of TM mode. The results show that the compact PBS based on silicon nitride nanowire assisted waveguide and grooved waveguide has excellent performance on LNOI platform. And this PBS can tolerate large manufacturing errors.

Table 1. Comparison of PBSs based on the LNOI platform.

Source	PER (dB)	IL (dB)	Length (μm)	BandWidth (nm)	Cut
[4]	~21 (TE) ~45 (TM)	<1 (TE&TM)	>6000	150 (>20 dB, TE) 250 (>40 dB, TM)	x-cut
[5]	-	~2.8 (TE) ~1.3 (TM)	51000	140 (>20 dB, TE) 140 (>18 dB, TM)	z-cut
[6]	47.7 (TE) 48 (TM)	0.9 (TE) 0.6 (TM)	~430	over 200 (>17.8 dB, TE) over 200 (>22.8 dB, TM)	x-cut
[7]	~24 (TE) ~31 (TM)	0.3 (TE) 1.0 (TM)	160	185 (>20 dB, TE) 85 (>20 dB, TM)	z-cut
[12]	22.8 (TE) 26.2 (TM)	0.12 (TE) 0.47 (TM)	61.5	38 (>20 dB, TE&TM)	z-cut
[13]	26.7 (TE) 21.3 (TM)	<0.05 (TE&TM)	16	140 (>10 dB, TE&TM)	z-cut
[14]	~36(TE) ~35(TM)	1.10 (TE) 1.24(TM)	~180	50 (>10 dB, TE) 50 (>35 dB, TM)	z-cut
This work	40.7 (TE) 50.7 (TM)	<0.05 (TE&TM)	46	100(>10 dB, TE) 100(>45 dB, TM)	x-cut

2. Materials and Methods

Figure 1a,b respectively present schematics of the top and cross-sectional views of the proposed PBS. The device consists of two WGs (WG1, WG2) with coupling gap G. WG1 is a Si_3N_4 nanowire assisted waveguide and it ends with a through-output port. WG2 is a grooved-waveguide ending with a cross output port. The S-shaped curved waveguide with length L_s is used to decouple WG1 and WG2. The thickness of LN layer is 500 nm and embedded SiO_2 layer (box) is 2 μm. The waveguide height h_w is 300 nm, and SiO_2 is covered on the upper layer to protect WGs. The refractive indices of LN, Si_3N_4 and SiO_2 are $n_{LN} = 2.21$, $n_{Si_3N_4} = 2.46$ (which is relatively larger as the fabrication of film deposition is PEVED) and $n_{SiO_2} = 1.44$ at the wavelength of 1550 nm, respectively.

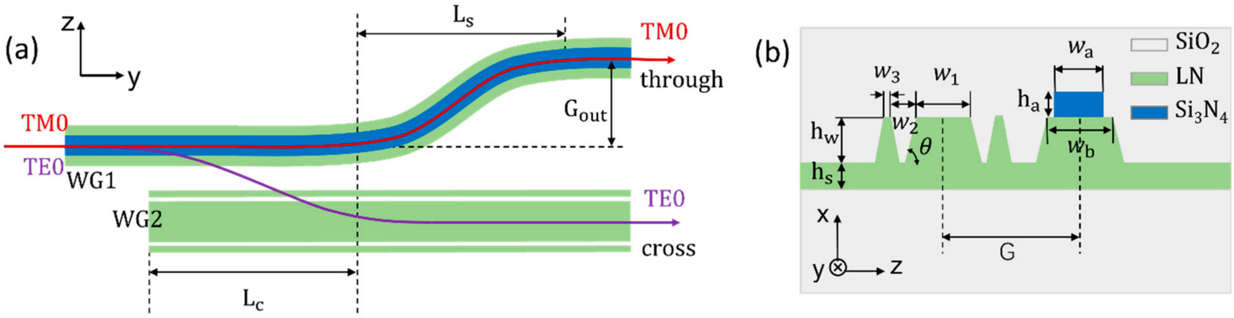

Figure 1. Schematics of proposed PBS; (**a**) top view and (**b**) cross-section view.

Although the Z-cut platform is more advantageous to design PBS, the existing LNOI electro-optic modulators are generally manufactured based on the X-cut platform to take advantage of the high electro-optic coefficient of the Z-axis. Considering that PBS will be integrated with modulators in the future, our design is based on X-cut LNOI platform [21]. LN WGs can be patterned with high resolution using Electron Beam Lithography (EBL) and Inductively Coupled Plasma Reactive Ion Etching (ICP-RIE). Limited by the manufacturing process, the side wall of LN WG manufactured by ICP-RIE inclines about 75° [22]. Therefore, we set the sidewall corner (θ) at 75° to match the manufacturing process.

By optimizing the geometric parameters (w_a, h_a) of Si_3N_4 nanowires, the effective refractive index (Neff) of TM_0 mode can be significantly improved, while the Neff of TE_0 mode can be slightly improved. Then, by optimizing the parameters (w_1, w_2, w_3) of grooved LN WG, the TE polarization can meet the phase matching condition, and there is a large phase mismatch of TM polarization, to significantly inhibit the cross-coupling of TM polarization. In this case, TE and TM can be separated after going through a short coupling region.

When the Si_3N_4 nanowires are loaded on LN WGs, the electric fields of TE polarization (whose main electrical field is horizontal) and TM polarization (whose main electrical field is vertical) will be affected differently. Figure 2a shows the Neff of TE_0 and TM_0 in Si_3N_4 assisted LNWG at the wavelength of 1.55 μm. We use Lumerical Finite Difference Eigenmode (FDE) solver to calculate their Neff. In the calculation, w_b is fixed at 600 nm. It can be seen that for both polarizations, Neff increases with w_a and h_a. However, with the increase of h_a, Neff of TM_0 will approach and exceed Neff of TE_0 eventually. According to Figure 2b, we choose (w_a, h_a) = (400, 500) nm, to match the Neff of TE_0 of grooved WG (~1.93), and to significantly increase Neff of TM_0. Figure 2c shows the relevant electric field distribution of TM_0 and TE_0 modes in the case of (w_a, h_a) = (400, 500) nm.

When the LN WGs are grooved, TE_0 and TM_0 will also be affected differently. Figure 3a shows the Neff of TE_0 and TM_0 modes in grooved LNWG at 1.55 μm wavelength. We also use the Lumerical FDE solver to calculate their Neff. In the calculation, w_1 is fixed at 1μm. And we assume that when w_2 is narrow, WG cannot be etched completely, but small pits are formed on the WG [23]. It can be seen that for both modes, Neff of grooved waveguide first increases and then decreases with the increase of w_2, and gradually approaches Neff of single-mode WG with the width w_1. So it is convenient for us to design Neff of TE polarization. According to Figure 3a, we select (w_2, w_3) as (200, 100) nm to exact match Neff of TE_0 mode. Figure 3b shows the electric field of TM_0 and TE_0 modes in the case of (w_2, w_3) = (200, 100) nm.

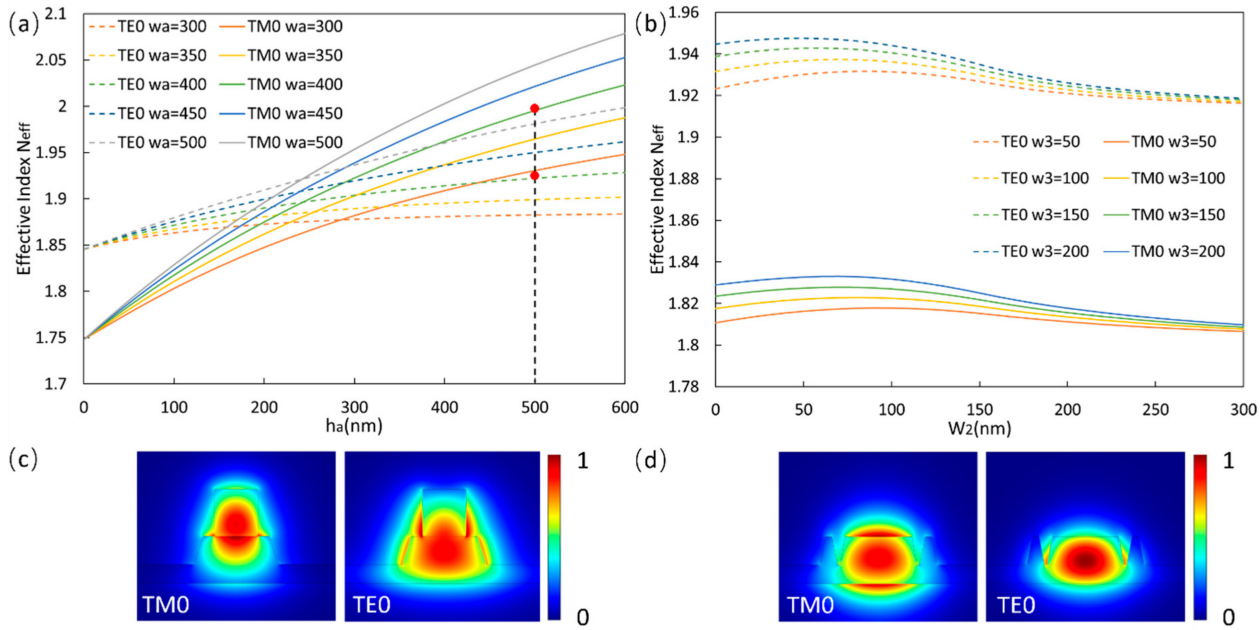

Figure 2. (**a**) Calculated effective indices of TE_0 and TM_0 modes in Si_3N_4 assisted LN WGs as a function of ha for different w_a. (**b**) Calculated effective indices of TE_0 and TM_0 modes in grooved LN WGs as a function of w_2 for different w_3. (**c**) Electrical field profiles for TM_0 mode (w_a, h_a) = (400, 500) nm, TE_0 mode (w_a, h_a) = (400, 500) nm. (**d**) Electrical field profiles for TM_0 mode (w_2, w_3) = (200, 100) nm, TE_0 mode (w_2, w_3) = (200, 100) nm.

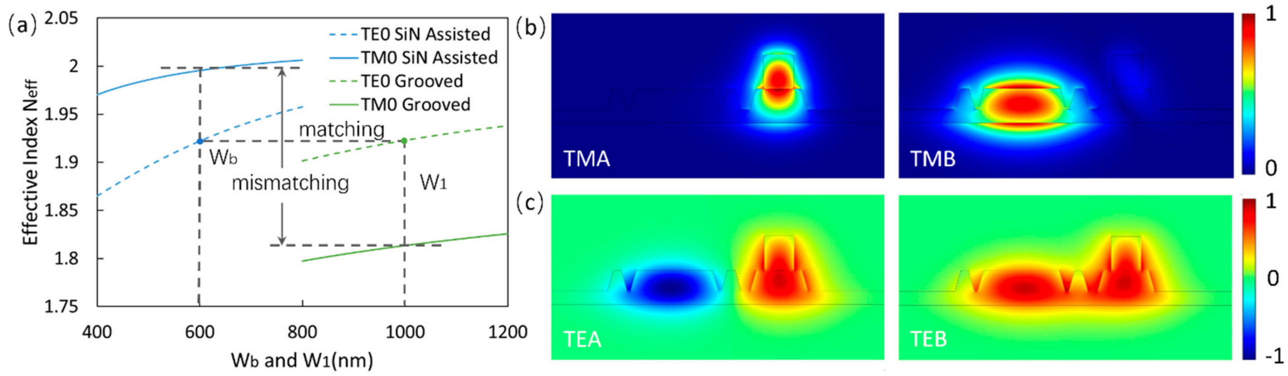

Figure 3. (**a**) Calculated effective index of TE_0 and TM_0 modes in Si3N4 assisted LN WGs and grooved LN WGs as a function of WG width. Electrical field profiles of (**b**) two quasi-TM super-modes, and of (**c**) odd and even TE super-modes in the coupling region.

Then, we calculate the Neff as a function of the width of WG at 1.55 µm wavelength, as shown in Figure 3 We choose w_1 as 1µm and w_b as 600 nm. As expected, the TE_0 meets the phase matching condition, while the Neff of TM_0 is significantly different.

3. Results

Lumerical 3D finite-difference time-domain (FDTD) is applied to further simulate the light transmission characteristics of the proposed structure. Cross-coupling length of TE_0 mode is determined by G. The smaller G is, the smaller coupling length of the DC is. However, undesired TM polarization cross-coupling will also increase due to the insufficient phase-mismatch caused by smaller G. Therefore, G is optimized to 1380 nm. w_a is optimized to 393 nm to obtain the maximum ER of TE_0. Considering the complete coupling of TE_0 mode, L_c is optimized to 36 µm. And G_{out} is set to 2 µm to avoid accidental coupling between two WGS. L_s is set to 10µm to ensure a low bending loss.

Figure 4a,b show the light propagation profiles of TE_0 and TM_0 at 1.55 µm, respectively. It can be seen that TE_0 is completely coupled with the cross port, while TM_0 has almost no coupling. The Extinction Ratio (ER) of TE_0 is 40.7 dB (mainly propagates from the cross port), while TM_0 is 50.7 dB (mainly propagates from the through port). For both polarizations, ultra-low Insertion Loss (IL < 0.05 dB) can be achieved. ER and IL are defined as follows:

$$ER_{TE} = 10\log_{10}\left(\frac{T_{cross,TE}}{T_{through,TE}}\right) \quad (1)$$

$$ER_{TM} = 10\log_{10}\left(\frac{T_{through,TM}}{T_{cross,TM}}\right) \quad (2)$$

$$IL_{TE} = 10\log_{10}(T_{cross,TE}) \quad (3)$$

$$IL_{TM} = 10\log_{10}\left(T_{through,TM}\right) \quad (4)$$

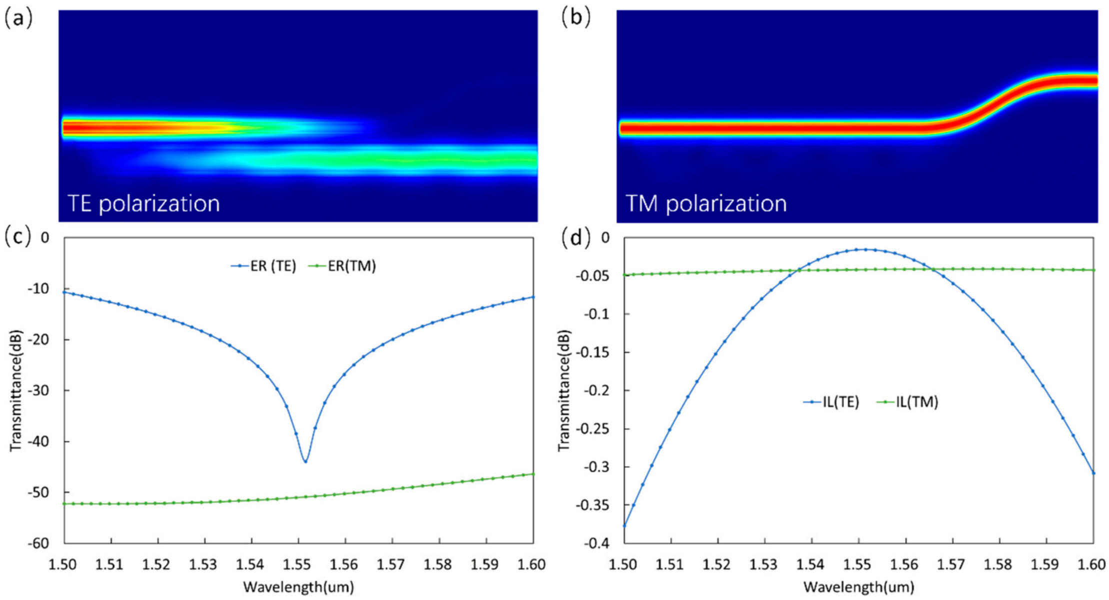

Figure 4. Light propagation profiles of (**a**) TE polarization and (**b**) TM polarization at the wavelength of 1550 nm; ER and IL of (**c**) TE polarization and (**d**) TM polarization as wavelength varies.

$T_{through}$ and T_{cross} are the through port and cross port transmission, respectively. Figure 4c,d show ERs and ILs of TE and TM polarization, respectively. It can be observed that for both polarizations, our PBS shows broadband performance with ERs > 10 dB over 100 nm wavelength ranges. In the wavelength range of 100 nm, the IL of TE polarization is less than 0.4 dB, and that of TM polarization is less than 0.05 dB The ILs of TM polarization is mainly caused by bending, which can be further reduced by increasing L_s.

The manufacturing tolerance is considered of four parameters, that is, (1) Etching depth error of grooves on LN film δh, (because narrow grooves are difficult to etch), (2) the sidewall angle of WGs δθ, (3) width of WGs δw (assuming that the two WGS have the same change), (4) mask misalignment δm (mask misalignment will cause the horizontal position of Si_3N_4 nanowires to shift). And Figure 5 shows the transmission spectrum of the corresponding parameters deviating from the optimized value. For both polarizations, When the range of δh/δθ/δw/δm is 30 nm/±3°/±20 nm/±30 nm, ER > 10 dB and IL < 0.5 dB of TE_0 and ER > 40 dB and IL < 0.05 dB of TM_0 can still be maintained in the 160 nm bandwidth. It is worth noting that TM_0 is much less sensitive to fabrication errors and wavelength changes than TE_0, which is caused by the large phase mismatch of TM_0.

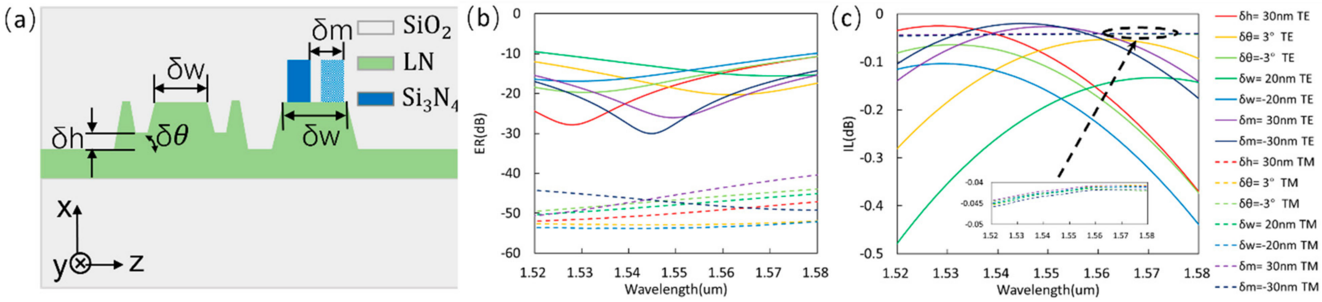

Figure 5. (**a**) Four parameters of manufacturing tolerance. (**b**) ERs and (**c**) ILs of the device with parameters deviating from the optimized value.

4. Discussion

In fact, single LN WG is easier to manufacture than grooved LN WG. We have tried to use single LN WG instead of grooved waveguide to build PBS as in reference [13]. However, there are few parameters that can be changed for a single LN WG. So it is difficult to design the Neff, resulting in poor extinction ratio. The groove waveguide we propose has three parameters that can be flexibly adjusted (w1, w2 and w3) to precisely design Neff of TE_0 and TM_0. Therefore, replacing LN WG with groove waveguide can make Neff of TE match better and Neff of TM difference larger, thus improving extinction ratio.

5. Conclusions

In this paper, we propose a compact, high extinction ratio, and low loss PBS based on an asymmetric directional coupler on LNOI platform. Si_3N_4 nanowires are deposited on LN waveguides to significantly change birefringence. By properly designing Si_3N_4 nanowires and grooved LN WGS, TE polarization meets the phase matching condition. However, TM polarization has an obvious phase mismatch, and the coupling is fully suppressed. We design a PBS with a length of 46 µm (including S-bend). Simulations show that the PBS has an ultra-high extinction ratio (ER) of TE_0 and TM_0 (larger than 40 dB and 50 dB, respectively). Simulation shows that PBS has the broadband performance of keeping ERs > 10 dB in the 100 nm wavelength range. In addition, PBS shows ultra-low IL (<0.05 dB) and maintains ILs < 0.4 dB in the 100 nm wavelength range. This device has good manufacturing error tolerance. We believe that our work paves the way for the integrated polarization control system on the LNOI platform.

Author Contributions: Conceptualization, J.T. and X.L.; methodology, J.T. and S.D.; software, J.T. and X.L.; validation, J.T. and X.L.; formal analysis, Y.Z. and C.W.; writing—original draft preparation, J.T.; writing—review and editing, J.L. (Jinye Li) and Y.Z.; project administration, J.L. (Jianguo Liu). X.L. and J.L. (Jinye Li) has made equal contributions to this work. All authors have read and agreed to the published version of the manuscript.

Funding: This research was funded by National Natural Science Foundation of China (NSFC), grant number 61727815, and 61731014.

Conflicts of Interest: The authors declare no conflict of interest.

References

1. Wang, C.; Zhang, M.; Chen, X.; Bertrand, M.; Shams-Ansari, A.; Chandrasekhar, S.; Winzer, P.; Loncar, M. Integrated lithium niobate electro-optic modulators operating at CMOS-compatible voltages. *Nature* **2018**, *562*, 101–104. [CrossRef] [PubMed]
2. Zhang, Y.; Wang, X.; Li, Z.; Lyu, W.; Lyu, Y.; Zeng, C.; Zhang, Z.; Zhang, S.; Zhang, Y.; Li, H.; et al. Flat Optical Frequency Comb Generation Based on Monolithic Integrated LNOI Intensity and Phase Modulator. *Photonics* **2022**, *9*, 495. [CrossRef]
3. Wang, J.; Chen, P.; Dai, D.; Liu, L. Polarization coupling of x-cut thin film lithium niobate based waveguides. *IEEE Photon. J.* **2020**, *12*, 2200310. [CrossRef]
4. Yang, G.; Sergienko, A.; Ndao, A. Plasmonic loss-mitigating broadband adiabatic polarizing beam splitter. *Opt. Lett.* **2022**, *47*, 629–632. [CrossRef]

5. Chung, H.; Lee, C.; Huang, K.; Yang, S.; Wang, K.; Solntsev, A.; Sukhorukov, A.; Setzpfandt, F.; Chen, Y. Broadband on-chip polarization mode splitters in lithium niobate integrated adiabatic couplers. *Opt. Express* **2019**, *27*, 1632–1645. [CrossRef]
6. Xu, H.; Dai, D.; Liu, L.; Shi, Y. Proposal for an ultra-broadband polarization beam splitter using an anisotropy-engineered Mach-Zehnder interferometer on the x-cut lithium-niobate-on-insulator. *Opt. Express* **2020**, *28*, 10899–10908. [CrossRef]
7. Deng, C.; Lu, M.; Sun, Y.; Huang, L.; Wang, D.; Hu, G.; Zhang, R.; Yun, B.; Cui, Y. Broadband and compact polarization beam splitter in LNOI hetero-anisotropic metamaterials. *Opt. Express* **2021**, *29*, 11627–11634. [CrossRef]
8. Dai, D. Advanced passive silicon photonic devices with asymmetric waveguide structures. *Proc. IEEE* **2018**, *106*, 2117–2143. [CrossRef]
9. Fukuda, H.; Yamada, K.; Tsuchizawa, T.; Watanabe, T.; Shinojima, H.; Itabashi, S.I. Ultrasmall polarization splitter based on silicon wire waveguides. *Opt. Express* **2006**, *14*, 12401–12408. [CrossRef]
10. Wu, H.; Tan, Y.; Dai, D. Ultra-broadband high-performance polarizing beam splitter on silicon. *Opt. Express* **2017**, *25*, 6069. [CrossRef]
11. Dai, D.; Bowers, J.E. Novel ultra-short and ultra-broadband polarization beam splitter based on a bent directional coupler. *Opt. Express* **2011**, *19*, 18614–18620. [CrossRef]
12. Jiang, R.; Xu, Y.; Dong, Y.; Zhang, B.; Ni, Y. Integrated TM-through/TE-converted polarization beam splitter based on z-cut lithium niobate-on-insulator platform. *Optik* **2022**, *255*, 168690. [CrossRef]
13. Zhang, L.; Zhang, L.; Fu, X.; Yang, L. Compact, Broadband and Low-Loss Polarization Beam Splitter on Lithium-Niobate-On-Insulator Using a Silicon Nanowire Assisted Waveguide. *IEEE Photon. J.* **2020**, *12*, 6601906. [CrossRef]
14. Wu, Y.; Sun, X.; Li, H.; Lu, C.; Zhang, Y.; Liu, S.; Zheng, Y.; Chen, X. Lithium Niobate Thin Film Polarization Beam Splitter Based on Asymmetric Directional Coupling. *J. Lightwave Technol.* **2022**, 1–5. [CrossRef]
15. Oulton, R.F.; Sorger, V.J.; Genov, D.A.; Pile, D.F.P.; Zhang, X. A hybrid plasmonic waveguide for subwavelength confinement and long-range propagation. *Nat. Photon.* **2008**, *2*, 496–500. [CrossRef]
16. Dai, D.; He, S. A silicon-based hybrid plasmonic waveguide with a metal cap for a nano-scale light confinement. *Opt. Express* **2009**, *17*, 16646–16653. [CrossRef]
17. Lou, F.; Dai, D.; Wosinski, L. Ultracompact polarization beam splitter based on a dielectric-hybrid plasmonic dielectric coupler. *Opt. Lett.* **2012**, *37*, 3372–3374. [CrossRef]
18. Chee, J.; Zhu, S.; Lo, G.Q. CMOS compatible polarization splitter using hybrid plasmonic waveguide. *Opt. Express* **2012**, *20*, 25345–25355. [CrossRef]
19. Guan, X.; Wu, H.; Shi, Y.; Wosinski, L.; Dai, D. Ultracompact and broadband polarization beam splitter utilizing the evanescent coupling between a hybrid plasmonic waveguide and a silicon nanowire. *Opt. Lett.* **2013**, *38*, 3005–3008. [CrossRef]
20. Almeida, V.R.; Xu, Q.; Barrios, C.A.; Lipson, M. Guiding and confining light in void nanostructure. *Opt. Lett.* **2004**, *29*, 1209–1211. [CrossRef]
21. Liu, H.; Guo, H.; Tan, M.; Li, Z. Research progress of lithium niobate thin-film modulators. *Chin. Opt.* **2022**, *15*, 1–13. [CrossRef]
22. Zhang, M.; Wang, C.; Cheng, R.; Shams-Ansari, A.; Lonar, M. Monolithic ultra-high-Q lithium niobate microring resonator. *Optica* **2017**, *4*, 1536–1537. [CrossRef]
23. Wu, B.; Kumar, A.; Pamarthy, S. High aspect ratio silicon etch: A review. *J. Appl. Phys.* **2010**, *108*, 051101. [CrossRef]